JACS
JOURNAL OF THE AMERICAN CHEMICAL SOCIETY
Article
pubs.acs.org/JACS

Highly Selective and Efficient Removal of Heavy Metals by Layered Double Hydroxide Intercalated with the MoS_4^{2-} Ion

Lijiao Ma,[†] Qing Wang,[†] Saiful M. Islam,[‡] Yingchun Liu,[†] Shulan Ma,*[,†,‡] and Mercouri G. Kanatzidis*[,‡]

[†]Beijing Key Laboratory of Energy Conversion and Storage Materials and College of Chemistry, Beijing Normal University, Beijing 100875, China

[‡]Department of Chemistry, Northwestern University, 2145 Sheridan Road, Evanston, Illinois 60208, United States

Supporting Information

ABSTRACT: The MoS_4^{2-} ion was intercalated into magnesium−aluminum layered double hydroxide (MgAl—NO_3-LDH) to produce a single phase material of $Mg_{0.66}Al_{0.34}(OH)_2(MoS_4)_{0.17}\cdot nH_2O$ (MgAl—MoS_4-LDH), which demonstrates highly selective binding and extremely efficient removal of heavy metal ions such as Cu^{2+}, Pb^{2+}, Ag^+, and Hg^{2+}. The MoS_4-LDH displays a selectivity order of Co^{2+}, Ni^{2+}, Zn^{2+} < Cd^{2+} ≪ Pb^{2+} < Cu^{2+} < Hg^{2+} < Ag^+ for the metal ions. The enormous capacities for Hg^{2+} (~500 mg/g) and Ag^+ (450 mg/g) and very high distribution coefficients (K_d) of ~10^7 mL/g place the MoS_4-LDH at the top of materials known for such removal. Sorption isotherm for Ag^+ agrees with the Langmuir model suggesting a monolayer adsorption. It can rapidly lower the concentrations of Cu^{2+}, Pb^{2+}, Hg^{2+}, and Ag^+ from ppm levels to trace levels of ≤1 ppb. For the highly toxic Hg^{2+} (at ~30 ppm concentration), the adsorption is exceptionally rapid and highly selective, showing a 97.3% removal within 5 min, 99.7% removal within 30 min, and ~100% removal within 1 h. The sorption kinetics for Cu^{2+}, Ag^+, Pb^{2+}, and Hg^{2+} follows a pseudo-second-order model suggesting a chemisorption with the adsorption mechanism via M—S bonding. X-ray diffraction patterns of the samples after adsorption demonstrate the coordination and intercalation structures depending on the metal ions and their concentration. After the capture of heavy metals, the crystallites of the MoS_4-LDH material retain the original hexagonal prismatic shape and are stable at pH ≈ 2−10. The MoS_4-LDH material is thus promising for the remediation of heavy metal polluted water.

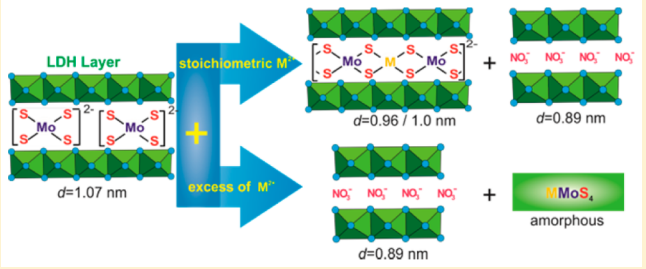

INTRODUCTION

Water contamination by toxic heavy metals such as Hg^{2+}, Pb^{2+}, and Cd^{2+} is becoming an increasingly important issue in separation science and environmental remediation,[1] because these metals are harmful to humans and other species.[2−4] Increasing amounts of mercury are discarded into the environment (air, soil, and water) due to its use in the pharmaceutical and paper industries, electric battery production, amalgam dental fillings, combustion of coal or oil, and etc. Effective reduction of Hg^{2+} and other heavy metals down to trace levels (e.g., < 5 ppb) remains a great challenge.[5] Conventional methods including chemical precipitation, flocculation, membrane separation, ion exchange, evaporation are suboptimal because of low capacities and low removal rates for metals other than Hg^{2+}. Precipitation employing sulfide ions cannot reduce the concentrations of heavy metals below acceptable drinking levels.[6] Adsorption method is considered to be quite attractive in terms of the low cost, simple design and strong operability, especially its high removal efficiency from dilute solutions.[7] Various materials such as zeolites,[8] activated carbon,[9−11] polymers,[12] biomaterials,[13] and sorption resins have been employed for the adsorption of metal ions.[14] Clays are also attractive as natural adsorbents because of their promise of low cost, high surface area, and hydrophilicity,[15,16] but they suffer from low selectivity and weak affinity for heavy metals. In spite of these, new highly efficient and cheaper adsorbents attract the attention of researchers.

Sulfides form strong covalent bonds with heavy metals,[17−24] and this can be the basis for designing effective adsorbent materials for their effective capture. Consequently, many crystalline sulfide-based materials have been well studied for remediation of heavy metal polluted water.[25−31] Our group has reported layered metal sulfides such as $K_{2x}Mn_xSn_{3-x}S_6$ (KMS-1),[32−35] $H_{2x}Mn_xSn_{3-x}S_6$ (LHMS-1),[36,37] $K_{2x}Mg_xSn_{3-x}S_6$ (KMS-2),[38,39] $K_{2x}Sn_{4-x}S_{8-x}$ (KTS-3),[40] and porous amorphous glass ($A_2A'_{2-x}$-$SnSb_2S_6$, A = Na; A′ = K, Cs),[41] all of which demonstrate high efficiency in removing heavy metals. Fu et al. studied the effects of pH, reaction time, initial concentration, reaction temperature and coexisting ions on the adsorption of Cu^{2+} by KMS-1.[42] These materials operate under the soft−hard Lewis acid−base paradigm mentioned above for the metal ion's selectivity.

The layered double hydroxides (LDHs) are anionic clays with positively charged host layers and counter-anions found in the interlayer space. The excellent intercalation and anion-

Received: January 5, 2016
Published: January 31, 2016

DOI: 10.1021/jacs.6b00110
J. Am. Chem. Soc. 2016, 138, 2858−2866

exchange properties[43] allow the LDHs versatile applications such as on catalysts,[44,45] two-dimensional nanoreactors,[39,46] adsorbents, and scavengers.[47,48] Given the many attractive features of this class of crystalline clay materials, we hypothesize that if we functionalize them with sulfide-containing groups, then we can combine the key advantages from two disparate kinds of materials (oxides and sulfides) into a single phase with enhanced built-in heavy metal removal properties. Recently, we introduced polysulfide anions $[S_x]^{2-}$ into the LDH gallery[49−52] and found that the as-formed composites were very effective in selective capture for heavy metals.[49,52] These materials, however, exhibit medium term instabilities associated with the oxidation of the $[S_x]^{2-}$ species to $[SO_4]^{2-}$.

Herein, we investigate the introduction of $(MoS_4)^{2-}$ into the MgAl-LDH interlayer structure and its heavy metal capture ability. The as-prepared MoS_4-LDH phase exhibits enormous selectivity for Ag^+ and Hg^{2+} ($K_d \approx 10^7$ mL/g), excellent removal capacity (~432 mg/g for Ag^+, ~500 mg/g for Hg^{2+}), and also fast trapping for them, placing it at the top materials for heavy metal removal among others. More importantly, the ability to diminish the heavy metal pollutant concentrations down to <5 ppb levels makes the MoS_4-LDH material attractive for environmental remediation applications.

EXPERIMENTAL SECTION

Materials. The MgAl—NO_3-LDH was prepared through NO_3^-/CO_3^{2-} ion-exchange reaction using MgAl—CO_3-LDH as a precursor based on refs 53−56. The $(NH_4)_2MoS_4$ was purchased from Sigma-Aldrich and used without further purification. The $(MoS_4)^{2-}$ anion coming from the red $(NH_4)_2MoS_4$ precursor was exchanged with NO_3^- anion of the white NO_3-LDH to obtain the red brown MoS_4-LDH. Typically, 0.2 g NO_3-LDH and 0.2 g $(NH_4)_2MoS_4$ were dispersed in 10 mL degassed deionized water, and the obtained suspension was allowed to react under stirring at ambient temperature for 24 h. The resulting brown solids were filtered, washed with deionized water and then acetone, and finally air-dried, to get 0.24 g product with a yield of ~93%.

Heavy Metal Uptake Experiments. The heavy metal uptakes from aqueous solutions with various concentrations were studied using the batch method. The metal ions involved the eight ions of Co^{2+}, Ni^{2+}, Cu^{2+}, Zn^{2+}, Ag^+, Pb^{2+}, Cd^{2+}, and Hg^{2+} coming from their nitrate salts. After mixing the solid sorbents with the solutions for certain time, centrifugation was performed, and the metal concentrations in the supernatant solutions were determined using inductively coupled plasma-atomic emission spectroscopy (ICP-AES) or inductively coupled plasma-mass spectroscopy (ICP-MS) for extra low concentration (≤1 ppb). The adsorptive capacity was evaluated from the difference of metal concentrations in mother and supernatant solutions.

The distribution coefficient (K_d) is defined by the equation of $K_d = (V[(C_0 - C_f)/C_f])/m$, where C_0 and C_f are, respectively, the initial and equilibrium concentrations of M^{n+} (ppm, μg/mL) after the contact, V is the solution volume (mL), and m is the solid amount (g).[32] The % removal is calculated with the equation of $100 \times (C_0 - C_f)/C_0$. The removal capacity ($q_m$) is given by the equation: $q_m = 10^{-3} \times (C_0 - C_f) \cdot V/m$. The adsorption experiments were performed with V:m ratios of 860−6000 mL/g at ambient temperature.

For distinguishing the high selective ions of Cu^{2+}, Hg^{2+}, and Ag^+, experiments containing them all together were carried out. An ~10 ppm concentration for each ion (~30 ppm for total) was mixed with certain quantities of MoS_4-LDH (0.01 and 0.005 g), which was sufficient to pick up only one of the ions.

The experiments to investigate the removal capacity for certain ions such as Hg^{2+}, Ag^+, Cu^{2+}, and Pb^{2+} employed various concentrations were performed with the batch method (V/m = 860−1000 mL/g) at room temperature with 24 h of contact time. The data obtained were used for the determination of the sorption isotherms.

Adsorption Kinetic Study. Adsorption kinetic experiments for the ions of Cu^{2+}, Ag^+, Pb^{2+}, and Hg^{2+} under various adsorption times (5−300 min) were performed. For each operation, 0.035 g of solid sample was weighted into a 50 mL centrifugal tube, and a 30 mL aqueous solution containing certain ion (20−30 ppm) was added (V/m = 860 mL/g). At specified time intervals, the suspensions were centrifuged, and 2 mL of the supernatant solutions were taken and analyzed by ICP-AES and ICP-MS to get the ion contents.

Characterization Techniques. The XRD patterns of the as-prepared samples and those after adsorption experiments were collected using a PANalytical X'pert Pro MPD diffractometer with Cu—Kα radiation at room temperature, with step size of 0.0167°, scan time of 10s per step, and 2θ ranging from 4.5 to 70°. The generator setting is 40 kV and 40 mA. Fourier transformed infrared (FT−IR) spectra of the samples were recorded on a Nicolet-380 Fourier-Transform infrared spectrometer using the KBr pellet method. Raman spectra were recorded on a microscopic confocal Raman spectrometer, using a 633 nm He−Ne laser. SEM measurements were carried out using a Hitachi S-4800 microscope.

The metal ion concentrations in solutions before and after adsorption were measured using ICP-AES (Jarrel-ASH, ICAP-9000) and ICP-MS (NexION 300X) for much low concentrations. For determining the compositions of the solid samples, ICP-AES (~0.1 M HNO_3 solution was used to dissolve the solids) and CHN analyses using an Elementar Vario EL elemental analyzer were conducted.

RESULTS AND DISCUSSION

Synthesis and Characterization of the MoS_4-LDH Material. The MoS_4-LDH material was accomplished via the ion-exchange reaction of the NO_3^- in NO_3-LDH with $(MoS_4)^{2-}$ as shown in eq 1.

$$Mg_{0.66}Al_{0.34}(OH)_2(NO_3)_{0.34}\cdot xH_2O + 0.17(NH_4)_2MoS_4 \rightarrow Mg_{0.66}Al_{0.34}(OH)_2(MoS_4)_{0.17}\cdot xH_2O + 0.34NH_4NO_3 \quad (1)$$

The obtained MoS_4-LDH powder sample is brown in color, as shown in the photograph in Scheme 1. According to ICP and CHN analyses, a stoichiometric composition of $Mg_{0.66}Al_{0.34}(OH)_2(MoS_4)_{0.17}\cdot 0.8H_2O$ was obtained. Figure 1A shows the comparison of the XRD patterns of NO_3-LDH precursor and the exchanged product MoS_4-LDH. Compared with the 0.88 nm basal spacing (d_{basal}) of the NO_3-LDH (Figure 1A-a), the as-prepared MoS_4-LDH had an enlarged d_{basal} of 1.07 nm (Figure 1A-b), confirming the introduction of the larger $(MoS_4)^{2-}$ in the interlayer space. The (00l) reflections at 1.07, 0.53, and 0.36 nm indicate a layered phase. The weakened

Scheme 1. Ion Exchange and Reaction Scheme of MoS_4-LDH and the Binding Modes of $[MoS_4]^{2-}$ with M^{2+} at Different Concentration Regimes and Proposed Arrangements of Interlayer Species in LDH Gallery

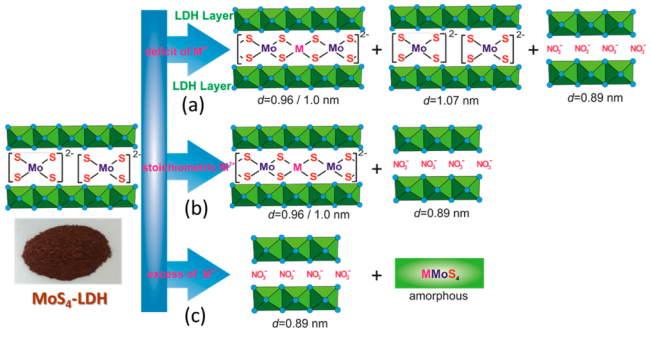

DOI: 10.1021/jacs.6b00110
J. Am. Chem. Soc. 2016, 138, 2858−2866

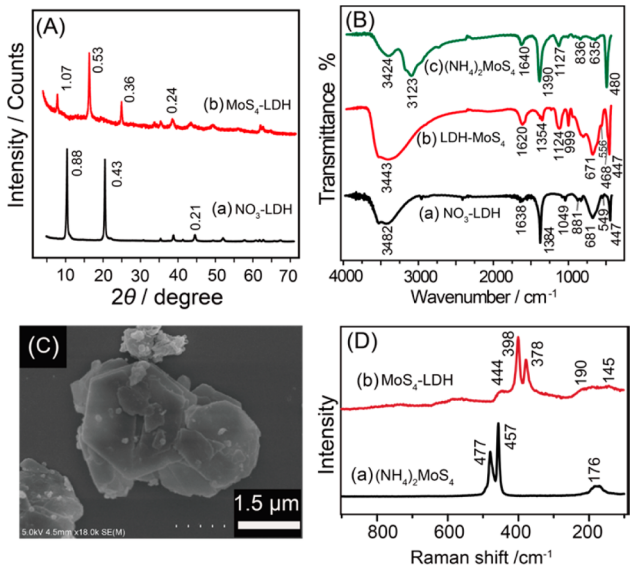

Figure 1. (A) XRD patterns of (a) NO_3-LDH and (b) MoS_4-LDH, (B) IR spectra of (a) NO_3-LDH, (b) MoS_4-LDH, and (c) $(NH_4)_2MoS_4$, (C) Typical SEM image of the MoS_4-LDH showing typical hexagonal shaped crystallites, and (D) Raman data of (a) $(NH_4)_2MoS_4$ and (b) MoS_4-LDH.

(003) reflection at 1.07 nm in comparison to the stronger (006) reflection at 0.53 nm results from the very heavy nature of the intercalated $(MoS_4)^{2-}$ anions and strong scattering property. This massive electron density on the (006) plane of the structure increases X-ray scattering from this plane.

IR spectroscopy (Figure 1B) verified the formation of the intercalated compound. In Figure 1B-a, the strong band appearing at 1384 cm^{-1} corresponds to the NO_3^- of the NO_3-LDH. When the $(MoS_4)^{2-}$ anions enter the gallery, the NO_3^- band at 1384 cm^{-1} diminishes (Figure 1B-b), suggesting an almost-complete exchange. For free $(NH_4)_2MoS_4$ (Figure 1B-c), the band at 480 cm^{-1} is assigned to the Mo—S vibration, consistent with reference values (459–482 cm^{-1}) for Mo—S stretching bands.[57,58] In MoS_4-LDH, the M—S band becomes indistinguishable, because of the overlap with the M—O bands at 447 cm^{-1} from the LDH layers.[59] The Raman spectra (Figure 1D) can give more detailed information on the Mo—S stretching bands. For $(NH_4)_2MoS_4$ (Figure 1D-a), there are two obvious peaks at 477 and 457 cm^{-1}, assigned to the Mo—S stretching bands, based on the reference values ranged in 400–510 cm^{-1}.[60] In MoS_4-LDH (Figure 1D-b), the Mo—S stretching bands appear at 444, 398, and 378 cm^{-1}, for which the red-shift would be attributed to the interaction of the intercalated MoS_4^{2-} ions with the LDH layer hydroxides likely through Mo—S···HO hydrogen bonding involving the hydroxide ions in the LDH. Generally, small and highly charged anions preferentially occupy the LDH interlayer space,[61−65] thus, the −2 charged $(MoS_4)^{2-}$ ions provide a strong driving force for the exchange over the singly charged NO_3^-. SEM image (Figure 1C) shows the hexagonal crystals of MoS_4-LDH which resemble the NO_3-LDH precursor, as found in our previous work.[49]

Heavy Metal Removal Using MoS_4-LDH. The uptake of heavy metal ions by MoS_4-LDH from solution in various concentrations was studied by the batch method at room temperature. The affinity of MoS_4-LDH toward these metal ions can be expressed in terms of the distribution coefficient K_d (for definition, see the Experimental Section). The adsorption experiments with individual solutions of Co^{2+}, Ni^{2+}, Cu^{2+}, Zn^{2+}, Ag^+, Pb^{2+}, Cd^{2+}, and Hg^{2+}, as well as solutions with all eight ions together were carried out. Table 1 summarizes the adsorption results for individual ions by MoS_4-LDH. The adsorption ability of MoS_4-LDH toward Hg^{2+} and Cu^{2+} is much higher than for the other ions. After 6 h contact time the concentrations of these ions decrease from the starting value of ~10 ppm to ≤1–2 ppb, achieving a nearly 100% removal. The Ag^+ and Pb^{2+} also display good removal efficiency, achieving >99.5% removal rates and $>10^5$ mL/g K_d values within 6 h contact time. In sharp contrast to the other two transition metal ions of Cu^{2+} and Zn^{2+}, the adsorptive capacity for Co^{2+} and Ni^{2+} was very low, which may provide a good method for separating these ions. This result is in agreement with our previous work.[49]

Table 1. Adsorption Results of MoS_4-LDH toward Individual Eight Ions (10 ppm)[a,b]

	initial solution		after 6 h adsorption			
single ions	C_0 (ppm)	pH	C_f −6h (ppm)	pH-6h	M^{n+} removal (%)	K_d (mL/g)
Co^{2+}	10.03	6.13	6.34	6.49	36.79	582
Ni^{2+}	10.13	5.83	5.40	6.47	46.69	876
Cu^{2+}	8.92	6.18	0.002	6.78	99.98	4.5×10^6
Zn^{2+}	9.26	6.24	0.16	7.38	98.27	5.7×10^4
Ag^+	8.96	5.74	0.044	7.28	99.51	1.7×10^5
Pb^{2+}	8.64	5.62	0.029	7.39	99.66	2.6×10^5
Cd^{2+}	9.36	6.68	0.57	6.73	93.91	1.3×10^4
Hg^{2+}	12.77	4.11	0.001	6.32	99.99	1.1×10^7

[a]ion concentration: ~ 10 ppm per ion. Contact time: 6 h. [b]V = 30 mL; m (mass of solid sample) = 0.030 g; V/m ratio = 30/0.030 = 1000.

Table 2 shows the results of competitive capture reactions for the case with all eight ions in the same solution (e.g., "mixed ion state"). The observed selectivity order for these ions was Co^{2+}, Ni^{2+}, Zn^{2+} < Cd^{2+} ≪ Pb^{2+} < Cu^{2+}, Ag^+, and Hg^{2+}. The K_d^{Hg} and K_d^{Ag} values are ~10^3 times larger than the K_d^{Pb} and ~10^5 larger than the K_d^{Cd}, reflecting the high preference for Hg^{2+}/Ag^+ over Pb^{2+}/Cd^{2+}. This indicates that MoS_4-LDH is very selective for ions with high Lewis acid softness (i.e., Hg^{2+}/Ag^+ vs Pb^{2+}/Cd^{2+}). The excellent adsorption for Cu^{2+}, Ag^+ and Hg^{2+} is in good agreement with those observed in single ion

Table 2. Adsorption of MoS_4-LDH toward the Eight Mixed Ions[a,b]

mixed ions	C_0 (ppm)	C_f −3h (ppm)	M^{n+} removal (%)	K_d (mL/g)
Co^{2+}	9.99	9.90	0.9	8
Ni^{2+}	10.20	10.10	1.0	9
Cu^{2+}	10.16	0.00078	100	1.1×10^7
Zn^{2+}	9.63	9.50	1.3	12
Ag^+	11.84	0.00048	100	2.1×10^7
Pb^{2+}	10.44	0.65	93.8	1.3×10^4
Cd^{2+}	9.99	8.18	18.1	190
Hg^{2+}	14.46	0.001	100	1.2×10^7
pH: 3.72→ 5.08				

[a]V = 30 mL; m = 0.030 g; V/m ratio =1000. [b]Concentration per ion: ~ 10 ppm. Contact time: 3 h.

DOI: 10.1021/jacs.6b00110
J. Am. Chem. Soc. 2016, 138, 2858–2866

Table 3. Selective Adsorption of MoS_4-LDH for Separating Cu^{2+}, Ag^+, and Hg^{2+}[a]

	0.005 g			0.01 g		
	Ag^+	Cu^{2+}	Hg^{2+}	Ag^+	Cu^{2+}	Hg^{2+}
C_0 (ppm)	10.76	10.45	11.89	10.76	10.45	11.89
C_f-3h (ppm)	0.52	10.45	4.37	0.006	9.46	0.03
K_d-3h (mL/g)	1.2×10^5	0	1.0×10^4	5.4×10^6	3.1×10^2	1.2×10^6
% removal	95.17	0	63.25	99.94	9.47	99.75
pH-3h	2.93→ 3.10			2.93→ 3.91		

[a]30 mL solution, 10 ppm per ion, 3h contact time.

adsorption, except for Zn^{2+} and Cd^{2+}. Here the adsorptions toward Zn^{2+} and Cd^{2+} decreased dramatically compared with that in single ion state. Compared to its single ion solution, the removal toward Ag^+ demonstrated a marked increase, with an augmentation of ~100 fold (= $2.1 \times 10^7/1.7 \times 10^5$) for K_d^{Ag}. A cooperative interaction of the coexisting ions seems responsible for the increase. Another reason may be the increased acidity of the mixed solution (pH = 3.7−5.1). The acidity may affect the hydration of certain ions to different degree, which can modulate their binding force with the $[MoS_4]^{2-}$ group.

Typically, materials with K_d values on the order of ~10^4-10^5 mL/g are considered to be exceptional adsorbents.[32,52,66] As shown in Table 2, for the highly toxic Hg^{2+}, the K_d^{Hg} value for MoS_4-LDH reaches ~10^7 mL/g. The K_d^{Hg} is higher than that found for our reported materials (10^3−10^6 mL/g) of KMS-2[38] and LHMS ($H_{2x}Mn_xSn_{3-x}S_6$),[37] close to our S_4-LDH material[49] and porous amorphous chalcogenides $A_2A'_{2-x}$-$SnSb_2S_6$ (~10^7 mL/g),[41] matching or exceeding those commercial resins (~10^4−5.1×10^5 mL/g),[67,68] the silane chelating fibers (3.0×10^5−3.8×10^6 mL/g),[69] chalcogel-1 (9.2×10^6−1.6×10^7 mL/g),[21] and thiol-functionalized silicates (3.4×10^5−1.0×10^8 mL/g).[27,67,70] The present MoS_4-LDH material may trap the metal ions by forming M-S coordination bonds as our reported S_x-LDH,[49] but the functionalized silica sorbents generally need incorporation of custom designed sulfur containing organic functional groups. Clearly, the present material can rapidly reduce the concentration of soft heavy metals in aqueous solution to very low levels. The Hg^{2+} concentration is always lower than 1 ppb, well below the acceptable level in drinking water (2 ppb).[70] These results highlight the strong potential of MoS_4-LDH as a highly effective filter for decontamination of water polluted with heavy metals.

Relative Selectivity for Cu^{2+}, Ag^+, and Hg^{2+}. As shown above, the MoS_4-LDH can capture the Cu^{2+}, Ag^+, and Hg^{2+} ions effectively, with their concentrations fast reduced from 10 ppm to ≤1 ppb (Table 2). We were interested to see if MoS_4-LDH has any preference among these three atoms that might become the basis for separating them. The ability to distinguish Ag^+ and Hg^{2+} from one another is especially important because such a challenging problem is often encountered in mining operations of precious metals.[38] From Table 2, we can see that Ag^+ and Hg^{2+} are so similar in their reactivity ($K_d \approx 10^7$ mL/g) that they cannot be selectively separated using the MoS_4-LDH under the employed operating conditions. In order to effectively separate Ag^+ from Hg^{2+} as well as Cu^{2+}, we conducted a solution containing the only three ions of Cu^{2+}, Ag^+, and Hg^{2+} in a 10 ppm concentration for each ion, and decreased quantities (0.01 and 0.005 g) of MoS_4-LDH were adequate for picking up only one of them. The results of these experiments are shown in Table 3.

The separation factor for A and B ($SF_{A/B}$) defined by K_d^A/K_d^B is a scale to determine whether a material can be used to separate out certain ions from one another.[39] Generally, good separation factors are considered to >100, depending on the conditions and applications for which the SF is measured. When using 0.01 g MoS_4-LDH (Table 3), the $SF_{Ag/Cu}$ and $SF_{Hg/Cu}$ values are both about 10 000, showing an obvious higher affinity for Ag^+ and Hg^{2+} than for Cu^{2+}. And also, the $SF_{Ag/Hg}$ of 5 suggests a somewhat higher selectivity toward Ag^+ than Hg^{2+}. Importantly enough, the almost-complete removal for the Ag^+ and Hg^{2+} when using the small quantity of 0.01 g further display the wonderful capture ability of MoS_4-LDH toward these two ions. When the sorbent amount was decreased to 0.005 g, the $SF_{Ag/Hg}$ was 12, suggesting only a modest separation factor for Ag^+ and Hg^{2+}. Thus, the three ions follow an exact selectivity order of $Ag^+ > Hg^{2+} \gg Cu^{2+}$.

Sorption Isotherm toward Ag^+ and Uptake Capacity for the Ions. From the results described above, the MoS_4-LDH shows the highest selectivity for Ag^+. The maximum adsorption capacity of the material was determined from an adsorption equilibrium study. The Ag^+ capture by MoS_4-LDH was found to increase successively with increasing concentration (10−1700 ppm, Table 4). Over a wide range of the initial concentration (10−400 ppm), the Ag^+ removal rates reached values of >98%, with the K_d^{Ag} values ranging from 4×10^4 to 3×10^7 mL/g. The maximum removal capacity (q_m) for Ag^+ reached ~452 mg/g. This is an exceptionally high capacity competing with the best absorbers such as S_4-LDH (383 mg/g)[49] and KMS-2 (408 mg/g)[38] and magnetic cellulose xanthate,[71] for which adsorption capacities of various adsorbents are shown in Table 5.[33,37,38,49,72−82]

Table 4. Sorption Isotherm Data of MoS_4-LDH towards Ag^+[a]

C_0 (ppm)	C_f (ppm)	pH-initial	pH-24h	removal (%)	q_m (mg/g)	K_d (mL/g)
9.52	0	5.90	7.43	100	8.2	
38.58	0.001	5.75	6.84	100	33.2	3.3×10^7
83.68	0.02	5.12	6.72	99.98	71.9	3.6×10^6
404	9.52	4.48	6.54	97.64	339.3	3.6×10^4
747	300	3.80	4.77	59.84	384.4	1.3×10^3
1038	519	3.56	4.63	50.00	446.3	8.6×10^2
1174	678	3.33	4.65	42.25	426.6	6.3×10^2
1338	870	3.49	4.80	34.98	402.5	4.6×10^2
1484	958	3.45	5.09	35.44	452.4	4.7×10^2
1685	1159	3.13	4.85	31.22	452.4	3.9×10^2

[a]m = 0.035 g, V= 30 mL, V/m = 860 mL/g. Contact time: 24 h.

MoS_4-LDH can extract silver ranging from trace levels to highly concentrated solution with excellent efficiency. We also checked the adsorption of the MoS_4-LDH material for Hg^{2+} in the range of concentrations 40 ppm to 500 ppm (Table S1), and found that there are >99.9% removal rates in all cases and a

DOI: 10.1021/jacs.6b00110
J. Am. Chem. Soc. 2016, 138, 2858−2866

Table 5. Comparison of Adsorption Capacities of Various Adsorbents for Heavy Metal Ions

target ions	adsorbents	q_m (mg/g)	refs
Cu^{2+}	MoS_4-LDH	181	this work
	TA-HTC[a]	81	ref 72
	Cl-LDH[b]	38	ref 73
	H100-LDH[c]	85	ref 73
	edta-LDH[d]	71	ref 74
	LS-LDH[e]	64	ref 75
	S_x-LDH[f]	127	ref 49
	PANI−PS[g]	171	ref 76
	KMS-1[h]	156	ref 42
Pb^{2+}	MoS_4-LDH	290	this work
	Cl-LDH	40	ref 77
	DTPA-LDH[i]	170	ref 77
	H100-LDH	99	ref 73
	edta-LDH	180	ref 74
	MNP−CTS[j]	140	ref 78
	CDpoly-MNPs[k]	65	ref 79
	LS-LDH	123	ref 75
	Fe_3O_4-GS[l]	28	ref 80
Hg^{2+}	MoS_4-LDH	500	this work
	mercaptosuccinic acid−LDH[m]	161	ref 81
	KMS-2[n]	297	ref 38
	PANI−PS	148	ref 76
	MNPs-DTC[o]	48	ref 82
	KMS-1	377	ref 33
	LHMS-1[p]	87	ref 37
	Fe_3O_4-GS	23	ref 80
Ag^+	MoS_4-LDH	450	this work
	S_x-LDH	383	ref 49
	KMS-2	408	ref 38
	MCX[q]	166	ref 71

[a]Hydrotalcite modified by tannin (TA-HTC). [b]Layered double hydroxides intercalated by chloride (Cl-LDH). [c]MgAl layered double hydroxide (MgAl-LDH) intercalated by humate anions. [d]ZnAl layered double hydroxide (ZnAl-LDH) intercalated with edta. [e]MgAl-LDH intercalated by sulfonated lignin (LS). [f]MgAl-LDH intercalated by polysulfide $[S_x]^{2-}$. [g]Polyaniline−polystyrene composite (PANI−PS). [h]Layered metal sulfides of $K_{2x}Mn_xSn_{3-x}S_6$. [i]MgAl-LDH intercalated with diethylenetriamine-pentaacetic acid (DTPA). [j]Multiwalled carbon nanotubes coated with magnetic amino-modified $CoFe_2O_4$ ($CoFe_2O_4$—NH_2) nanoparticles (MNPs) further modified with chitosan (CTS). [k]Carboxymethyl-β-cyclodextrin (CM-β-CD) polymer modified Fe_3O_4 nanoparticles (CDpoly-MNPs). [l]Magnetic Fe_3O_4 and graphene composite functionalized by amino (Fe_3O_4-GS). [m]MgAl-LDH intercalated by mercaptocarboxylic acid. [n]Layered metal sulfides of $K_{2x}Mg_xSn_{3-x}S_6$. [o]Magnetic nanoparticles (MNPs) of Fe_3O_4 functionalized by dithiocarbamate (DTC). [p]Layered hydrogen metal sulfide (LHMS) of $H_{2x}Mn_xSn_{3-x}S_6$. [q]Magnetic cellulose xanthate (MCX).

~500 mg/g maximum adsorption capacity. For Pb^{2+}, in the concentration range of 10 ppm to 1000 ppm (Table S2), the MoS_4-LDH has a maximum adsorption capacity of ~290 mg/g. For Cu^{2+}, the maximum adsorption capacity is found to be relatively lower at ~181 mg/g (Table S3), however this value is still very high compared to reported adsorbents.[49,72−75] In comparison to the reported LDH intercalates or other materials as shown in Table 5, the present MoS_4-LDH demonstrates superior removal capacities for the target ions, which is attributed to the function of the introduced $(MoS_4)^{2-}$ ions in the LDH gallery.

As described above, the MoS_4-LDH has a chemical formula of $Mg_{0.66}Al_{0.34}(OH)_2(MoS_4)_{0.17}\cdot 0.8H_2O$, with a molecular weight of 110, so 1 g of MoS_4-LDH has 0.00154 (= 1/110 × 0.17) moles of $(MoS_4)^{2-}$. If the binding ratio of Ag:(MoS_4) is 2, then the theoretical combined Ag^+ amount will be 0.334 g (= 0.00154 × 2 × 108) and the theoretical maximum capacity 334 mg/g. The larger experimental value of ~452 mg/g observed suggests that the hydroxide-containing LDH layers can also adsorb some Ag^+. We did the control experiments using just the NO_3-LDH precursor as an adsorbent, and found the NO_3-LDH surely adsorbed some Ag^+, with a 15% removal rate under the concentration of 1700 ppm, which means the Ag^+ ion may bind to the hydroxide groups of the LDH layers as well.

A Langmuir isotherm is used to describe the experimental data of Ag^+. In this model, the adsorbate moieties (Ag^+ ions) are assumed to undergo monolayer type coverage of the sorbent on an adsorbent surface. Once an adsorption site is occupied, no further adsorption can happen at the same site. The Langmuir isotherm model is listed as eq 2:

$$q = q_m \frac{bCe}{1 + bCe} \tag{2}$$

where q (mg/g) is the equilibrium adsorption capacity of Ag^+ adsorbed, c_e (mg/L) is the Ag^+ concentration at equilibrium, q_m (mg/g) is the theoretical maximum sorption capacity. The equilibrium adsorption isotherm is shown in Figure 2, with the

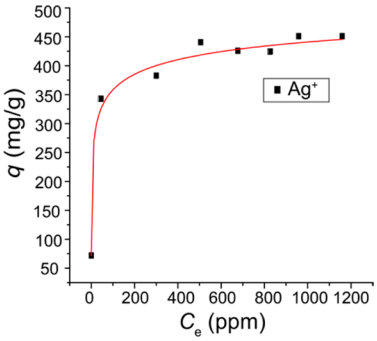

Figure 2. Sorption isotherm for the sorption of Ag^+ by MoS_4-LDH. The Langmuir equilibrium isotherm (red line) is derived from the Ag^+ equilibrium concentration (C_e), plotted against the capacity of q (mg/g).

Ag^+ equilibrium concentration ranging from 0.02 to 1200 ppm. The data points were well-fitted with the Langmuir model to determine the q_m of 545 mg/g, which is 1.2 times (= 545/452) of the experimental value of 452 mg/g. The large correlation coefficient (R^2 > 0.97) shows a good fit with the Langmuir isotherm, suggesting a monolayer adsorption[82,83] on the MoS_4-LDH.

Adsorption Kinetics Study. The adsorption kinetics of the Cu^{2+}, Ag^+, Pb^{2+}, and Hg^{2+} ions by MoS_4-LDH was also investigated in order to study adsorption rate and pathways of adsorption until equilibrium was reached. As depicted in Table 6, Tables S4−S6, and Figure 3A,3B, the adsorption rates for the ions of Hg^{2+}, Cu^{2+}, Ag^+, and Pb^{2+} were found to be very rapid. Within 5 min, the MoS_4-LDH achieved ≥97% removal rates and K_d values of >10^4 mL/g for Ag^+ (Table S5) and Hg^{2+} (Table 6). Within 30 min, the MoS_4-LDH achieved ≥99.7% removal rates and K_d values of >10^5 mL/g for Ag^+, Hg^{2+} and Pb^{2+} (Table S5, Table 6, Table S6). For the Cu^{2+} ion, the adsorption is slightly slow but still has a 98.5% removal rate in

DOI: 10.1021/jacs.6b00110
J. Am. Chem. Soc. 2016, 138, 2858−2866

Table 6. Kinetics Data of Hg^{2+} Adsorption using MoS_4-LDH[a]

C_0 (ppm)	time (min)	C_f (ppm)	removal (%)	K_d (mL/g)	q_t(mg/g)
27.1	5	0.74	97.27	3.1×10^4	22.67
	30	0.07	99.74	3.3×10^5	23.25
	60	0.05	99.82	4.7×10^5	23.26
	120	0.02	99.93	1.2×10^6	23.29
	180	0.004	99.99	5.8×10^6	23.30
	240	0.003	99.99	7.8×10^6	23.30
	300	0.002	99.99	1.2×10^7	23.30

[a] m = 0.035 g, V = 30 mL, V:m = 860 mL/g.

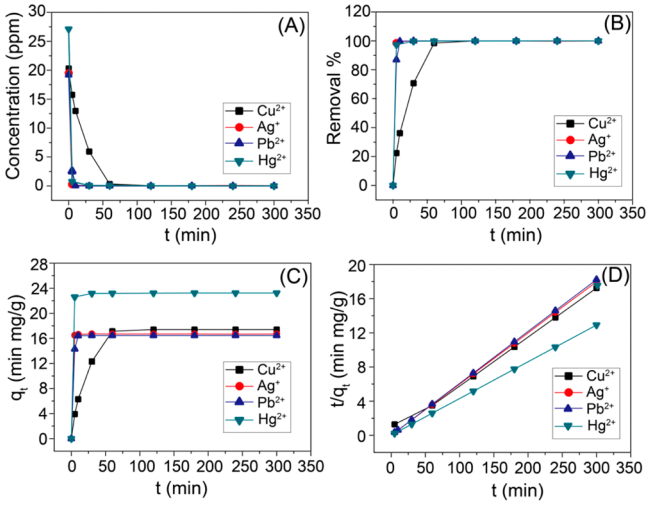

Figure 3. Adsorption kinetics curves for Cu^{2+}, Ag^+, Pb^{2+} and Hg^{2+}: (A) Ion concentration change following contact time, (B) Removal % as a function of contact time, (C) Sorption capacity (q_t) with contact time, (D) Pseudo-second-order kinetic plots for ion sorption.

1h. The adsorptions for all of the four ions reach equilibrium within ~1 h (Figure 3B,3C). For the Hg(II) adsorption, a similar kinetics trend was observed in previous studies,[38,82,84] but the adsorption of those materials is not so efficient and fast as the present material. The removal rate for Hg^{2+} herein is also faster than those found for polymer-brush-functionalized magnetic nanoparticles (MNPs).[82] The rate of adsorption was determined by using two different rate equations. Pseudo-first-order and pseudo-second-order mechanisms were investigated for determining adsorption behaviors. The comparison was then drawn between the experimental and calculated data. The two kinetic rate equations can be written as follows:[85]

Pseudo-first-order:

$$\ln(q_e - q_t) = \ln q_e - k_1 t \quad (3)$$

Pseudo-second-order:

$$\frac{t}{q_t} = \frac{1}{k_2 q_e^2} + \frac{t}{q_e} \quad (4)$$

where q_e (mg/g) is the amount of Hg^{2+} adsorbed per unit mass of adsorbent at equilibrium, and q_t (mg/g) is the Hg^{2+} adsorbed at time t, while k_1 (min^{-1}) and k_2 (g/mg min^{-1}) are equilibrium rate constants of pseudo-first-order and pseudo-second-order adsorption interactions, respectively. The k_1 value was obtained by plotting $\ln(q_e$-$q_t)$ against t and the k_2 value by plotting t/q_t against t. All the kinetic parameters for the adsorptions toward the four ions of Cu^{2+}, Ag^+, Hg^{2+}, and Pb^{2+} are summarized in Table 7. Moreover, the linear relationship of t/q_t versus t is presented in Figure 3D. From the kinetic parameters in Table 7, the calculated sorption capacities ($q_{e,cal}$) derived from the pseudo-second order model are closer to corresponding experimental values ($q_{e,exp}$). The goodness of fit coefficient (R^2) close to 1 indicates the adsorption for these ions by MoS_4-LDH can be well-described with a pseudo-second order kinetic model, suggesting the process is essentially a chemisorption.[86]

Table 7. Kinetic Parameters (Pseudo-Second-Order-Model) For Adsorbing Metal Ions onto MoS_4-LDH

	$q_{e,exp}$	k_2	$q_{e,cal}$ mg/g	R^2
Cu^{2+}	17.40	5.58×10^{-3}	18.18	0.998
Ag^+	16.70	2.24	16.69	1
Pb^{2+}	16.45	0.271	16.47	1
Hg^{2+}	23.24	0.362	23.26	1

Structural Characterization and Morphologies after Metal Ion Adsorption. After adsorption, the suspentions were centrifuged, and the solid samples were dried to conduct XRD, IR analyses, and SEM observations. As shown in Figure 4, in the case of low metal concentrations of 10 ppm, the samples after adsorption for various ions showed diverse XRD patterns. The samples with low adsorbed amount such as for Co^{2+} and Ni^{2+} (Figure 4a,b) displayed the d_{basal} values of 1.07 nm, similar to the MoS_4-LDH precursor (Figure 1A-b). The samples with high adsorption capacities such as for Cu^{2+} and Ag^+ revealed mainly d_{basal} values of 0.96 nm (Figure 4c,e), which is smaller than the d_{basal} (1.07 nm) of the MoS_4-LDH precursor. The new basal spacing at 0.96 nm may be attributed to the coordination of the adsorbed ions with the $(MoS_4)^{2-}$ groups. Here since the amount of metal ions is small compared to great excess of MoS_4-LDH, the $[M(MoS_4)_2]$ anionic complexes may be formed, which remain in the LDH interlayer giving a new d_{basal} of 0.96 nm. When the ion concentration levels are high such as in the case of 1500 ppm Ag^+, neutral salts

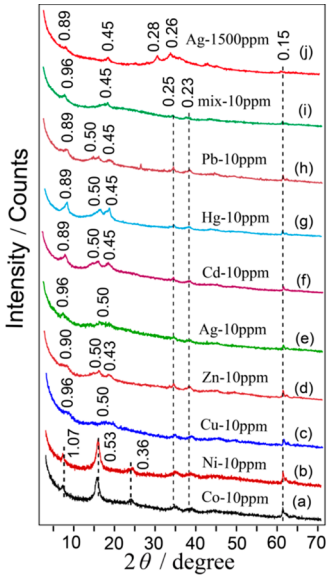

Figure 4. XRD patterns of samples after MoS_4-LDH adsorbed 10 ppm of (a) Co^{2+}, (b) Ni^{2+}, (c) Cu^{2+}, (d) Zn^{2+}, (e) Ag^+, (f) Cd^{2+}, (g) Hg^{2+}, and (h) Pb^{2+}, (i) Mixed solution of eight ions with a 10 ppm for each ion, and (j) 1500 ppm Ag^+.

DOI: 10.1021/jacs.6b00110
J. Am. Chem. Soc. 2016, 138, 2858−2866

such as amorphous Ag_2MoS_4 can form, which exited the gallery, and NO_3^- anions entered into it, making the characteristic 0.89 nm d_{basal} reflection of LDH-NO_3 dorminant (Figure 4j). The samples after adsorption of the Cd^{2+}, Hg^{2+}, and Pb^{2+} ions showed similar XRD patterns (Figure 4f–h), having with an obvious d_{basal} value of 0.89 nm as well as another possible d_{basal} of 1.0 nm, as deduced from the 0.5 nm (006) Bragg peak. The coexistence of the two d_{basal} values of 0.89 and 1.0 nm suggest the presence of two phases: the LDH(NO_3) and the $[M(MoS_4)_2]^{n-}$ intercalated LDH. The appearance of 1.0 nm/0.96 nm d_{basal} in different ions may be owing to their different coordiantion motifs with the $(MoS_4)^{2-}$ group.

The adsorption and stability of MoS_4-LDH were also confirmed by the IR spectra (Figure 5). A band at 1385

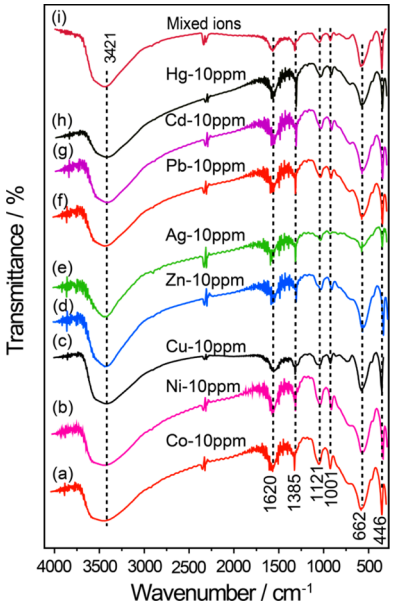

Figure 5. IR spectra of samples obtained after MoS_4-LDH adsorbed the 10 ppm (a) Co^{2+}, (b) Ni^{2+}, (c) Cu^{2+}, (d) Zn^{2+}, (e) Ag^+, (f) Pb^{2+}, (g) Cd^{2+}, (h) Hg^{2+}, and (i) their mixed solution.

cm^{-1} occurred for all solid samples after the adsorption, implying the presence of NO_3^- anions, which accompanied the metal ion entrance into the adsorbent for charge balance. The unchanged ν(M—O) vibrations at 662 cm^{-1} and δ(O—M—O) modes at 446 cm^{-1}[159] indicate the stability of the LDH layer undergoing the adsorption process. The samples after metal adsorption retained the hexagonal prismatic morphology (Figure 6), consistent with that of the MoS_4-LDH precusor (Figure 1C).

Binding Modes of $(MoS_4)^{2-}$ with M^{n+} and Guest Arrangements within LDH Gallery. Structural changes in the MoS_4-LDH samples after the adsorption were suggested by XRD as discussed above. On the basis of the above observations and the complexation chemistry of $(MoS_4)^{2-}$,[87−89] the mechanisms of metal capture are summarized as follows:

1. At low contents of metal ions, where the MoS_4-LDH is in large excess, the following reaction (eq 5) appears to dominate the adsorption process:

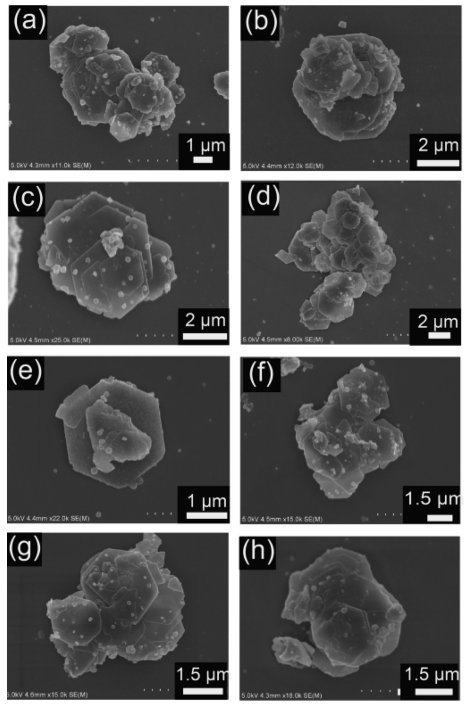

Figure 6. SEM images of the solid samples after MoS_4-LDH adsorbed 10 ppm (a) Co^{2+}, (b) Ni^{2+}, (c) Cu^{2+}, (d) Ag^+, (e) Cd^{2+}, (f) Hg^{2+}, (g) Pb^{2+}, and (h) their mixed solutions with a 10 ppm concentration for each ion.

$$\text{LDH-}[(MoS_4)^{2-}]_x + yM(NO_3)_2 \rightarrow \text{LDH-}[(MoS_4)^{2-}]_{x-2y} + \text{LDH-}\{[M(MoS_4)_2]^{2-}\}_y(NO_3^-)_{2y}(x \gg y) \quad (5)$$

Here we assume the M^{n+} ions have a −2 charge. In this case, because the $(MoS_4)^{2-}$ anions are in large excess relative to M^{2+}, more $(MoS_4)^{2-}$ would combine with less M^{2+} to form anionic complexes such as $[M(MoS_4)_2]^{2-}$ ions, which retain in the LDH interlayer. Because $x \gg y$, the dominant interlayer anions are still $[MoS_4]^{2-}$ with the resulting d_{basal} of 1.07 nm (Scheme 1a).

2. When the metal ions are in medium quantities, the capture processe may be described by Scheme 1b and eq 6:

$$\text{LDH-}[(MoS_4)^{2-}]_x + yM(NO_3)_2 \rightarrow \text{LDH-}\{[M(MoS_4)_2]^{2-}\}_{x/2} + \text{LDH-}(NO_3^-)_{2y}(x = 2y) \quad (6)$$

In this case, the amount of $(MoS_4)^{2-}$ is still in excess compared with M^{2+}, so the anionic complex $[M(MoS_4)_2]^{2-}$ is dorminant, with the d_{basal} values of 0.96 or 1.0 nm depending on the different size of the coordinated ions. The closer x and y values result in the coexistence of the two phases as shown in Scheme 1b.

3. When the metal ions are in excess of amounts, the capture can be described by eq 7:

$$\text{LDH-}[(MoS_4)^{2-}]_x + yM(NO_3)_2 \rightarrow \text{LDH-}(NO_3^-)_{2y} + xM(MoS_4)(x = y) \quad (7)$$

Here the LDH-$[(MoS_4)^{2-}]_x$ would be saturated by coordination with the adsorbed metal ions. Thus,

DOI: 10.1021/jacs.6b00110
J. Am. Chem. Soc. 2016, 138, 2858−2866

amorphous neutral salts of $M(MoS_4)$ should be formed accompanied by the NO_3^- intercalated phase (Scheme 1c).

CONCLUSIONS

The hybrid material of MoS_4-LDH forms readily from the insertion of the $(MoS_4)^{2-}$ ion in the interlayer space of LDH using ion-exchange chemistry. On the basis of the soft Lewis base nature of the sulfide ions in MoS_4^{2-} ion, the MoS_4-LDH material exhibits substantial uptake and excellent selectivity for a variety of soft Lewis acid heavy metal ions. After heavy metal uptake, the materials retain their original hexagonal prismatic crystallite shape, indicating good chemical stability. When all ions are copresent in aqueous solution (so-called mixed ion state), the selectivity order is Co^{2+}, Ni^{2+}, $Zn^{2+} < Cd^{2+} \ll Pb^{2+} < Cu^{2+}$, Hg^{2+}, Ag^+. In a solution containing mixtures of the three ions of Cu^{2+}, Hg^{2+}, and Ag^+, the selectivity order of $Cu^{2+} < Hg^{2+} < Ag^+$ was observed using MoS_4-LDH as a limiting reagent. The MoS_4-LDH can adsorb certain ions with extremely high adsorption capacities (~452 mg/g for Ag^+ and 500 mg/g for Hg^{2+}), and trap them rapidly even when present at trace levels. For the highly toxic Hg^{2+}, exceptionally rapid capture (~99.7% removal within 30 min at a 30 ppm concentration) was observed and final concentrations well below the acceptable levels in drinking water (<5 ppb) were achieved. The pseudo-second-order model describes well the adsorption behavior toward the ions of Cu^{2+}, Ag^+, Pb^{2+}, and Hg^{2+}, indicating a chemisorption process which occurs via M—S bonding. Therefore, we suggest the MoS_4-LDH material as highly efficient system for the rapid decontamination of water polluted by heavy metals.

ASSOCIATED CONTENT

Supporting Information

The Supporting Information is available free of charge on the ACS Publications website at DOI: 10.1021/jacs.6b00110.

Sorption data of MoS_4-LDH toward Hg^{2+}, Pb^{2+}, and Cu^{2+} in different concentration, kinetics data for adsorbing Cu^{2+}, Ag^+, and Pb^{2+} (PDF)

AUTHOR INFORMATION

Corresponding Authors

*mashulan@bnu.edu.cn

*m-kanatzidis@northwestern.edu

Author Contributions

The manuscript was written through contributions from all authors. All authors have given approval to the final version of the manuscript.

Notes

The authors declare no competing financial interest.

ACKNOWLEDGMENTS

This work is supported by the National Science Foundation of China (NSFC, No. 21271028) and the National Science Foundation grant DMR-1410169.

REFERENCES

(1) Hubner, R.; Astin, K. B.; Herbert, R. J. H. *J. Environ. Monit.* **2010**, *12*, 740.

(2) Carnizello, A. P.; Marcal, L.; Calefi, P. S.; Nassar, E. J.; Ciuffi, K. J.; Trujillano, R.; Vicente, M. A.; Korili, S. A.; Gil, A. *J. Chem. Eng. Data* **2009**, *54*, 241.

(3) Shannon, M. A.; Bohn, P. W.; Elimelech, M.; Georgiadis, J. G.; Marinas, B. J.; Mayes, A. M. *Nature* **2008**, *452*, 301.

(4) Schwarzenbach, R. P.; Escher, B. I.; Fenner, K.; Hofstetter, T. B.; Johnson, C. A.; von Gunten, U.; Wehrli, B. *Science* **2006**, *313*, 1072.

(5) Bhattacharyya, K. G.; Gupta, S. S. *Sep. Purif. Technol.* **2006**, *50*, 388.

(6) Tonini, D. R.; Gauvin, D. A.; Soffel, R. W.; Freeman, W. P. *Environ. Prog.* **2003**, *22*, 167.

(7) Wang, X. H.; Deng, W. Y.; Xie, Y. Y.; Wang, C. Y. *Chem. Eng. J.* **2013**, *228*, 232.

(8) Blanchard, G.; Maunaye, M.; Martin, G. *Water Res.* **1984**, *18*, 1501.

(9) Mohan, D.; Singh, K. P. *Water Res.* **2002**, *36*, 2304.

(10) Zhao, X. W.; Jia, Q.; Song, N. Z.; Zhou, W. H.; Li, Y. S. *J. Chem. Eng. Data* **2010**, *55*, 4428.

(11) Du, W.; Yin, L. B.; Zhuo, Y. Q.; Xu, Q. S.; Zhang, L.; Chen, C. H. *Ind. Eng. Chem. Res.* **2014**, *53*, 582.

(12) Liu, J. S.; Ma, Y.; Xu, T. W.; Shao, G. Q. *J. Hazard. Mater.* **2010**, *178*, 1021.

(13) Albadarin, A. B.; Al-Muhtaseb, A. H.; Al-laqtah, N. A.; Walker, G. M.; Allen, S. J.; Ahmad, M. N. M. *Chem. Eng. J.* **2011**, *169*, 20.

(14) Tharanitharan, V.; Srinivasan, K. *Asian J. Chem.* **2010**, *22*, 3036.

(15) Benhammou, A.; Yaacoubi, A.; Nibou, L.; Tanouti, B. *J. Colloid Interface Sci.* **2005**, *282*, 320.

(16) El Mouzdahir, Y.; Elmchaouri, A.; Mahboub, R.; ElAnssari, A.; Gil, A.; Korili, S. A.; Vicente, M. A. *Appl. Clay Sci.* **2007**, *35*, 47.

(17) Sutorik, A. C.; Kanatzidis, M. G. *J. Am. Chem. Soc.* **1997**, *119*, 7901.

(18) Muller, A.; Krickemeyer, E.; Wittneben, V.; Bogge, H.; Lemke, M. *Angew. Chem., Int. Ed. Engl.* **1991**, *30*, 1512.

(19) Shafaei-Fallah, M.; He, J. Q.; Rothenberger, A.; Kanatzidis, M. G. *J. Am. Chem. Soc.* **2011**, *133*, 1200.

(20) Ding, N.; Kanatzidis, M. G. *Nat. Chem.* **2010**, *2*, 187.

(21) (a) Bag, S.; Trikalitis, P. N.; Chupas, P. J.; Armatas, G. S.; Kanatzidis, M. G. *Science* **2007**, *317*, 490. (b) Kanatzidis, M. G. *Adv. Mater.* **2007**, *19*, 1165−1181.

(22) Bag, S.; Gaudette, A. F.; Bussell, M. E.; Kanatzidis, M. G. *Nat. Chem.* **2009**, *1*, 217.

(23) Oh, Y.; Morris, C. D.; Kanatzidis, M. G. *J. Am. Chem. Soc.* **2012**, *134*, 14604.

(24) Manos, M. J.; Chrissafis, K.; Kanatzidis, M. G. *J. Am. Chem. Soc.* **2006**, *128*, 8875.

(25) Mercier, L.; Pinnavaia, T. J. *Adv. Mater.* **1997**, *9*, 500.

(26) Brown, J.; Mercier, L.; Pinnavaia, T. J. *Chem. Commun.* **1999**, 69.

(27) Feng, X.; Fryxell, G. E.; Wang, L. Q.; Kim, A. Y.; Liu, J.; Kemner, K. M. *Science* **1997**, *276*, 923.

(28) Shin, Y. S.; Fryxell, G.; Um, W. Y.; Parker, K.; Mattigod, S. V.; Skaggs, R. *Adv. Funct. Mater.* **2007**, *17*, 2897.

(29) Riley, B. J.; Chun, J.; Ryan, J. V.; Matyáš, J.; Li, X. S.; Matson, D. W.; Sundaram, S. K.; Strachan, D. M.; Vienna, J. D. *RSC Adv.* **2011**, *1*, 1704.

(30) Figueira, P.; Lopes, C. B.; Daniel-da-Silva, A. L.; Pereira, E.; Duarte, A. C.; Trindade, T. *Water Res.* **2011**, *45*, 5773.

(31) Parham, H.; Zargar, B.; Shiralipour, R. *J. Hazard. Mater.* **2012**, *205*, 94.

(32) Manos, M. J.; Ding, N.; Kanatzidis, M. G. *Proc. Natl. Acad. Sci. U. S. A.* **2008**, *105*, 3696.

(33) Manos, M. J.; Kanatzidis, M. G. *Chem. - Eur. J.* **2009**, *15*, 4779.

(34) Manos, M. J.; Malliakas, C. D.; Kanatzidis, M. G. *Chem. - Eur. J.* **2007**, *13*, 51.

(35) Manos, M. J.; Kanatzidis, M. G. *J. Am. Chem. Soc.* **2012**, *134*, 16441.

(36) Manos, M. J.; Kanatzidis, M. G. *J. Am. Chem. Soc.* **2009**, *131*, 6599.

(37) Manos, M. J.; Petkov, V. G.; Kanatzidis, M. G. *Adv. Funct. Mater.* **2009**, *19*, 1087.

DOI: 10.1021/jacs.6b00110
J. Am. Chem. Soc. 2016, 138, 2858−2866

(38) Fard, Z. H.; Malliakas, C. D.; Mertz, J. L.; Kanatzidis, M. G. *Chem. Mater.* **2015**, *27*, 1925.
(39) Mertz, J. L.; Fard, Z. H.; Malliakas, C. D.; Manos, M. J.; Kanatzidis, M. G. *Chem. Mater.* **2013**, *25*, 2116.
(40) Sarma, D.; Malliakas, C. D.; Subrahmanyam, K. S.; Islam, S. M.; Kanatzidis, M. G. *Chem. Sci.* **2016**, *7*, 1121.
(41) Fard, Z. H.; Islam, S. M.; Kanatzidis, M. G. *Chem. Mater.* **2015**, *27*, 6189.
(42) Li, J. R.; Wang, X.; Yuan, B. L.; Fu, M. L. *J. Mol. Liq.* **2014**, *200*, 205.
(43) Khan, A. I.; O'Hare, D. *J. Mater. Chem.* **2002**, *12*, 3191.
(44) Constantino, V. R. L.; Pinnavaia, T. J. *Catal. Lett.* **1994**, *23*, 361.
(45) Corma, A.; Fornes, V.; Rey, F.; Cervilla, A.; Llopis, E.; Ribera, A. *J. Catal.* **1995**, *152*, 237.
(46) Gérardin, C.; Kostadinova, D.; Sanson, N.; Coq, B.; Tichit, D. *Chem. Mater.* **2005**, *17*, 6473.
(47) Rives, V.; Ulibarri, M. A. *Coord. Chem. Rev.* **1999**, *181*, 61.
(48) Xue, X. Y.; Gu, Q. Y.; Pan, G. H.; Liang, J.; Huang, G. L.; Sun, G. B.; Ma, S. L.; Yang, X. J. *Inorg. Chem.* **2014**, *53*, 1521.
(49) Ma, S. L.; Chen, Q. M.; Li, H.; Wang, P. L.; Islam, S. M.; Gu, Q. Y.; Yang, X. J.; Kanatzidis, M. G. *J. Mater. Chem. A* **2014**, *2*, 10280.
(50) Ma, S. L.; Islam, S. M.; Shim, Y.; Gu, Q. Y.; Wang, P. L.; Li, H.; Sun, G. B.; Yang, X. J.; Kanatzidis, M. G. *Chem. Mater.* **2014**, *26*, 7114.
(51) Ma, S. L.; Shim, Y.; Islam, S. M.; Subrahmanyam, K. S.; Wang, P. L.; Li, H.; Wang, S. C.; Yang, X. J.; Kanatzidis, M. G. *Chem. Mater.* **2014**, *26*, 5004.
(52) Ma, S. L.; Huang, L.; Ma, L. J.; Shim, Y.; Islam, S. M.; Wang, P. L.; Zhao, L. D.; Wang, S. C.; Sun, G. B.; Yang, X. J.; Kanatzidis, M. G. *J. Am. Chem. Soc.* **2015**, *137*, 3670.
(53) Iyi, N.; Matsumoto, T.; Kaneko, Y.; Kitamura, K. *Chem. Mater.* **2004**, *16*, 2926.
(54) Ma, S. L.; Fan, C. H.; Du, L.; Huang, G. L.; Yang, X. J.; Tang, W. P.; Makita, Y.; Ooi, K. *Chem. Mater.* **2009**, *21*, 3602.
(55) Ma, S. L.; Wang, J.; Du, L.; Sun, Y. H.; Gu, Q. Y.; Sun, G. B.; Yang, X. J. *J. Colloid Interface Sci.* **2013**, *393*, 29.
(56) Ma, S. L.; Du, L.; Wang, J.; Chu, N. K.; Sun, Y. H.; Sun, G. B.; Yang, X. J.; Ooi, K. *Dalton. Trans.* **2011**, *40*, 9835.
(57) Hibble, S. J.; Feaviour, M. R. *J. Mater. Chem.* **2001**, *11*, 2607.
(58) Weber, T.; Muijsers, J. C.; vanWolput, H. J. M. C.; Verhagen, C. P. J.; Niemantsverdriet, J. W. *J. Phys. Chem.* **1996**, *100*, 14144.
(59) Xu, Z. P.; Zeng, H. C. *J. Phys. Chem. B* **2001**, *105*, 1743.
(60) Clark, R. J. H.; Walton, J. R. *J. Chem. Soc., Dalton Trans.* **1987**, 1535.
(61) Ogawa, M.; Saito, F. *Chem. Lett.* **2004**, *33*, 1030.
(62) Miyata, S. *Clays Clay Miner.* **1983**, *31*, 305.
(63) Yamaoka, T.; Abe, M.; Tsuji, M. *Mater. Res. Bull.* **1989**, *24*, 1183.
(64) Nakato, T.; Kuroda, K.; Kato, C. *Chem. Mater.* **1992**, *4*, 128.
(65) Vermeulen, L. A.; Thompson, M. E. *Nature* **1992**, *358*, 656.
(66) Lehto, J.; Clearfield, A. *J. Radioanal. Nucl. Chem.* **1987**, *118*, 1.
(67) Chen, X. B.; Feng, X. D.; Liu, J.; Fryxell, G. E.; Gong, M. L. *Sep. Sci. Technol.* **1999**, *34*, 1121.
(68) Yantasee, W.; Warner, C. L.; Sangvanich, T.; Addleman, R. S.; Carter, T. G.; Wiacek, R. J.; Fryxell, G. E.; Timchalk, C.; Warner, M. G. *Environ. Sci. Technol.* **2007**, *41*, 5114.
(69) Liu, C. Q.; Huang, Y. Q.; Naismith, N.; Economy, J. *Environ. Sci. Technol.* **2003**, *37*, 4261.
(70) Liu, J.; Feng, X. D.; Fryxell, G. E.; Wang, L. Q.; Kim, A. Y.; Gong, M. L. *Adv. Mater.* **1998**, *10*, 161.
(71) Beyki, M. H.; Bayat, M.; Miri, S.; Shemirani, F.; Alijani, H. *Ind. Eng. Chem. Res.* **2014**, *53*, 14904.
(72) Anirudhan, T. S.; Suchithra, P. S. *Appl. Clay Sci.* **2008**, *42*, 214.
(73) Gonzalez, M. A.; Pavlovic, I.; Barriga, C. *Chem. Eng. J.* **2015**, *269*, 221.
(74) Perez, M. R.; Pavlovic, I.; Barriga, C.; Cornejo, J.; Hermosin, M. C.; Ulibari, M. A. *Appl. Clay Sci.* **2006**, *32*, 245.
(75) Huang, G. L.; Wang, D.; Ma, S. L.; Chen, J. L.; Jiang, L.; Wang, P. Y. *J. Colloid Interface Sci.* **2015**, *445*, 294.
(76) Alcaraz-Espinoza, J. J.; Chavez-Guajardo, A. E.; Medina-Llamas, J. C.; Andrade, C. A. S.; de Melo, C. P. *ACS Appl. Mater. Interfaces* **2015**, *7*, 7231.
(77) Liang, X. F.; Hou, W. G.; Xu, Y. M.; Sun, G. H.; Wang, L.; Sun, Y.; Qin, X. *Colloids Surf., A* **2010**, *366*, 50.
(78) Zhou, L. C.; Ji, L. Q.; Ma, P. C.; Shao, Y. M.; Zhang, H.; Gao, W. J.; Li, Y. F. *J. Hazard. Mater.* **2014**, *265*, 104.
(79) Badruddoza, A. M.; Shawon, Z. B.; Daniel, T. W. J.; Hidajat, K.; Uddin, M. S. *Carbohydr. Polym.* **2013**, *91*, 322.
(80) Guo, X. Y.; Du, B.; Wei, Q.; Yang, J.; Hu, L. H.; Yan, L. G.; Xu, W. Y. *J. Hazard. Mater.* **2014**, *278*, 211.
(81) Nakayama, H.; Hirami, S.; Tsuhako, M. *J. Colloid Interface Sci.* **2007**, *315*, 177.
(82) Farrukh, A.; Akram, A.; Ghaffar, A.; Hanif, S.; Hamid, A.; Duran, H.; Yameen, B. *ACS Appl. Mater. Interfaces* **2013**, *5*, 3784.
(83) Saha, B.; Das, S.; Saikia, J.; Das, G. *J. Phys. Chem. C* **2011**, *115*, 8024.
(84) Shan, C.; Ma, Z. Y.; Tong, M. P.; Ni, J. R. *Water Res.* **2015**, *69*, 252.
(85) Liu, T. T.; Yang, M.; Wang, T. X.; Yuan, Q. P. *Ind. Eng. Chem. Res.* **2012**, *51*, 454.
(86) Bhattacharya, A. K.; Naiya, T. K.; Mandal, S. N.; Das, S. K. *Chem. Eng. J.* **2008**, *137*, 529.
(87) Prasad, T. P.; Diemann, E.; Muller, A. *J. Inorg. Nucl. Chem.* **1973**, *35*, 1895.
(88) Muller, A.; Menge, R.; Prasad, T. P. *Z. Anorg. Allg. Chem.* **1972**, *391*, 107.
(89) Quagraine, E. K.; Georgakaki, I.; Coucouvanis, D. *J. Inorg. Biochem.* **2009**, *103*, 143.

DOI: 10.1021/jacs.6b00110
J. Am. Chem. Soc. 2016, 138, 2858−2866